Cation Specificity of Vacuolar NHX-Type Cation/H^+ Antiporters[1][OPEN]

Elias Bassil,[a,b] Shiqi Zhang,[a] Haijun Gong,[a,c] Hiromi Tajima,[a] and Eduardo Blumwald[a,2,3]

[a]Department of Plant Sciences, University of California, Davis, California 95616
[b]Horticultural Sciences Department and Tropical Research and Education Center, University of Florida, Homestead, Florida 33031
[c]College of Horticulture, Northwest A&F University, Yangling, 712100 Shaanxi, China

ORCID IDs: 0000-0001-8109-5758 (E.Ba.); 0000-0002-6449-6469 (E.Bl.).

Cation/H^+ (NHX-type) antiporters are important regulators of intracellular ion homeostasis and are critical for cell expansion and plant stress acclimation. In Arabidopsis (*Arabidopsis thaliana*), four distinct NHX isoforms, named AtNHX1 to AtNHX4, locate to the tonoplast. To determine the concerted roles of all tonoplast NHXs on vacuolar ion and pH homeostasis, we examined multiple knockout mutants lacking all but one of the four vacuolar isoforms and quadruple knockout plants lacking any vacuolar NHX activity. The *nhx* triple and quadruple knockouts displayed reduced growth phenotypes. Exposure to sodium chloride improved growth while potassium chloride was deleterious to some knockouts. Kinetic analysis of K^+ and Na^+ transport indicated that AtNHX1 and AtNHX2 are the main contributors to both vacuolar pH and K^+ and Na^+ uptake, while AtNHX3 and AtNHX4 differ in Na^+/K^+ selectivity. The lack of any vacuolar NHX activity resulted in no K^+ uptake, highly acidic vacuoles, and reduced but not abolished vacuolar Na^+ uptake. Additional K^+/H^+ and Na^+/H^+ exchange activity assays in the quadruple knockout indicated Na^+ uptake that was not H^+ coupled, suggesting the existence of an alternative, cation/H^+-independent, Na^+ conductive pathway in vacuoles. These results highlight the importance of NHX-type cation/H^+ antiporters in the maintenance of cellular cation homeostasis and in growth and development.

Key cellular processes needed for growth, development, and acclimation to environmental stress all rely on the regulation of intracellular ion homeostasis (Bassil and Blumwald, 2014). Ion homeostasis in different compartments of the endomembrane system is achieved by the compartment-specific activity of H^+-translocating enzymes such H^+-pumping ATPases (and pyrophosphatase in vacuoles) that establish the H^+-electrochemical potential and by secondary transporters that use this gradient to couple the passive transport of H^+ with the active uptake of ions against their electrochemical gradient (Blumwald et al., 1987; Martinoia et al., 2007; Amtmann and Leigh, 2010). Ion homeostasis maintains solute and water uptake that generate the turgor that, together with the coordinated delivery of membrane components and cell wall material through endomembrane trafficking, drive cell expansion. In plants, the active uptake of K^+ into the vacuole generates the turgor needed for cell expansion. In the cytosol, K^+ plays an important function as an enzyme activator and setting the electrical potential across the plasma membrane.

NHX-type cation/H^+ antiporters belong to the monovalent cation/H^+ antiporter group of transporters (Mäser et al., 2001; Sze and Chanroj, 2018). In plants, NHX antiporters are ubiquitous and catalyze the electroneutral exchange of H^+ for Na^+ or K^+. By virtue of their biochemical activity, endosomal NHXs control both the luminal uptake of K^+ and Na^+ and the pH of the compartments where they reside. Vacuolar NHXs regulate luminal pH by countering the acidity generated by H^+ pumps and essentially function as H^+ leaks to fine-tune luminal pH. Arabidopsis (*Arabidopsis thaliana*) contains six intracellular AtNHX isoforms (Bassil et al., 2012; Chanroj et al., 2012). AtNHX7 (SALT OVERLY SENSITIVE1) and AtNHX8 are closely related antiporters but reside on the plasma membrane and, accordingly, are not involved directly in the ion homeostasis of intracellular compartments. In Arabidopsis, AtNHX1 to AtNHX4 reside on the tonoplast (Bassil et al., 2011b; McCubbin et al., 2014), while two additional isoforms, AtNHX5 and AtNHX6, localize to trafficking compartments of the Golgi, trans-Golgi, and

[1]This work was supported in part by grants from the National Science Foundation (MCB-0343279, IOS-0820112, and MCB1157824) and the Will W. Lester Endowment, University of California, to E.Bl. H.G. was supported in part by the China Scholarship Council (201506305005).

[2]Author for contact: eblumwald@ucdavis.edu.
[3]Senior author.
The author responsible for distribution of materials integral to the findings presented in this article in accordance with the policy described in the Instructions for Authors (www.plantphysiol.org) is: Eduardo Blumwald (eblumwald@ucdavis.edu).

E.Ba. and E.Bl. conceived, designed, and developed most of the experiments; E.Ba., S.Z., H.G., and H.T. performed the experiments; E.Ba., S.Z., and E.Bl. analyzed and interpreted the data and drafted and revised the article.

[OPEN] Articles can be viewed without a subscription.
www.plantphysiol.org/cgi/doi/10.1104/pp.18.01103

late endosomes/prevacuolar compartments (Bassil et al., 2011a; Reguera et al., 2015). In all sequenced plant genomes reported to date, including early land species, multiple orthologs with sequence similarity to members of either the vacuolar or endosomal group have been identified (Bassil et al., 2012; Sze and Chanroj, 2018), suggesting that both functional groups (i.e. vacuolar and endosomal NHXs) have been conserved through evolution. The existence of multiple isoforms within each group also raises the question of why multiple isoforms exist and whether these are functionally redundant or may have distinct roles for plant growth and development.

NHXs have been implicated in numerous physiological processes that depend on vacuolar ion homeostasis. AtNHX1 and AtNHX2 are required for vacuolar pH homeostasis and the uptake of K^+ (Apse et al., 2003; Bassil et al., 2011b; Barragán et al., 2012), salt stress acclimation (Apse et al., 1999), osmotic adjustment (Barragán et al., 2012), stomatal regulation (Andrés et al., 2014), and flower development (Yoshida et al., 1995; Bassil et al., 2011b). A main emphasis of past research has been the role of NHXs in salt acclimation, with much work focused on the constitutive *NHX* overexpression to improve salinity tolerance by increasing the sequestration of Na^+ in vacuoles (Bassil et al., 2012). The experimental evidence strongly supports a role in Na^+ transport under saline conditions, but more recent functional studies also point to basic roles of vacuolar NHXs under nonsaline conditions that go beyond stress acclimation (Bassil and Blumwald, 2014). In addition to the compartmentation of Na^+ in the vacuole, NHXs may contribute to salinity tolerance by favorably adjusting cellular K^+ homeostasis under saline conditions (Ma et al., 2017; Wu et al., 2018).

The existence of four vacuolar NHX mutant isoforms in Arabidopsis makes the characterization of the function of individual isoforms difficult because of possible overlapping functions and the lack of clear phenotypes of single gene knockout mutants (Bassil et al., 2011a, 2011b). By creating functional knockout plants lacking three or all vacuolar NHXs, we studied the contribution of each isoform to overall vacuole ion homeostasis and assessed their growth phenotypes. Here, we used a combination of reverse genetics, ion transport, and physiology to reveal the transport properties of each vacuolar AtNHX isoform and their cation specificity.

RESULTS

Characterization of Multiple-Order Vacuolar *NHX* Knockouts

We sought to characterize the concerted role of all four vacuolar NHX-type antiporters on plant growth and development by generating multiple-order knockout mutants using available single T-DNA insertion lines of *AtNHX1*, *AtNHX2*, *AtNHX3*, and *AtNHX4*. We reasoned that since AtNHX1 to AtNHX4 colocalize to the vacuole (McCubbin et al., 2014), the generation of insertional knockout mutants lacking all but one functional vacuolar *NHX* would make it possible to investigate, in planta, the function of each vacuolar NHX independently of any background activity resulting from the remaining functional vacuolar isoforms. We began by obtaining independent single T-DNA insertion lines for each *NHX* gene (Supplemental Fig. S1), confirmed by genotyping, and backcrossed twice before advancing these lines in crosses to obtain double knockout mutants as described previously (Bassil et al., 2011b). The triple knockout mutants were generated by crossing double knockout mutants that shared common T-DNA insertions, such as *nhx1-1/2-1* (i.e. *nhx1-1 nhx2-1*) with *nhx2-1/4-1* to obtain *nhx1-1/2-1/4-1* and *nhx1-1/2-1* with *nhx1-1/3-1* to obtain *nhx1-1/2-1/3-1*. A diagram of the crossing strategy and the resulting multiple vacuolar *nhx* insertion knockout mutants is shown in Supplemental Figure S2A. The lack of expression of full-length *NHX1*, *NHX2*, *NHX3*, and *NHX4* in triple or quadruple knockout mutants was confirmed using reverse transcription PCR. Thus, only *NHX1* was expressed in *nhx2-1/3-2/4-1*, only *NHX2* was expressed in *nhx1-1/3-1/4-1*, and only the respective transcripts of *NHX3* and *NHX4* were detected in *nhx1-1/2-1/4-1* and *nhx1-1/2-1/3-1*. No detectable expression of any vacuolar *NHX* was noted in the quadruple knockout mutant *nhx1-1/2-1/3-1/4-1* (Supplemental Fig. S2B). To determine whether the expression of other *NHX* isoforms changed in the triple knockout mutant background, we also quantified the relative expression of each functional *NHX* isoform (i.e. wild-type copy of *NHX* without T-DNA) in all triple knockouts using reverse transcription quantitative PCR (RT-qPCR). The relative expression of functional *NHX* isoforms in triple knockout mutants was comparable to that of the wild type (Supplemental Fig. S3), as the respective expression of *NHX1*, *NHX2*, *NHX3*, or *NHX4* in the triple knockout mutant *nhx2/3/4*, *nhx1/3/4*, *nhx1/2/4*, or *nhx1/2/3* was between 0.8- and 1.05-fold of the same transcript expressed in the wild type.

To further corroborate any phenotypes obtained from T-DNA insertion lines, we also generated independent quadruple knockout mutants using CRISPR/Cas9-based gene editing (Supplemental Figs. S4 and S5). We used the double knockout mutant *nhx1-2/3-2* as the genetic background and targeted guide RNAs for editing separate targets of *NHX2* and *NHX4* (see "Materials and Methods"). Targeting *NHX2* and *NHX4* in *nhx1-1/3-2* was more feasible than generating an alternate *nhx2/4* knockout mutant because of the close proximity of *NHX2* and *NHX4* in the genome; thus, high linkage frequency between the two loci results in a low frequency of identifying an *nhx2/4* knockout mutant. Thirteen independent lines out of 59 T1 transgenic plants transformed with the CRISPR/Cas9 constructs had a short PCR fragment that resulted from the 1.2-kb deletion of *NHX2* and a 1-bp insertion in target D in *NHX4*, which caused a frame shift in the fourth exon

(Supplemental Fig. S5). These data indicated that the use of CRISPR/Cas9 to edit *NHXs* was feasible and resulted in bona fide knockout mutant plants lacking the full-length expression of vacuolar *NHXs* resembling those obtained from T-DNA insertion knockout mutants. Additional comparisons between the CRISPR and T-DNA insertion quadruple knockout mutants are presented and discussed below.

Plant Growth and Development Require Vacuolar NHX-Type Antiporters

The triple and quadruple T-DNA insertion knockout mutants displayed unique and diverse phenotypes, including reduced growth (Fig. 1). In *nhx2/3/4* plants, no significant growth reduction was seen in any of the growth conditions tested as compared with wild-type plants (Fig. 1, B and C), while in *nhx1/3/4* plants, a slight reduction in growth was observed similar to that of the single knockout mutant *nhx1* (Apse et al., 2003; Bassil et al., 2011b). The remaining two triple knockout mutants, *nhx1/2/4* and *nhx1/2/3*, bearing either functional *NHX3* or *NHX4* but lacking both *NHX1* and *NHX2*, displayed very severe growth phenotypes. *nhx1/2/4* plants were highly stunted, displaying more than 50% reduction in plant biomass and rosette diameter compared with wild-type plants, while *nhx1/2/3* knockout mutant rosette diameter was 65% of the wild type and dry weight was 73% of the wild type. Under all conditions tested, *nhx1/2/4* grew more poorly than the *nhx1/2/3* knockout mutant, suggesting that, in addition to *NHX1* and *NHX2*, *NHX4* may be more important to overall growth than *NHX3*. The quadruple T-DNA insertion knockout mutant *nhx1/2/3/4* displayed a phenotype similar to that of *nhx1/2/4* (i.e. reduced dry weight and smaller rosette diameter). In fact, phenotypically, the T-DNA quadruple knockout mutant *nhx1/2/3/4* and the triple knockout mutant *nhx1/2/4* were indistinguishable. *nhx1/2/3/4* knockout mutants obtained via CRISPR/Cas9-guided gene editing resulted in plants with growth and developmental abnormalities similar to the quadruple insertional T-DNA mutant (Supplemental Fig. S6), indicating that the phenotypes obtained were a consequence of the lack of functional vacuolar NHX antiporters. Collectively, the growth data indicated that the lack of *NHX3* and *NHX4*, when either *NHX1* or *NHX2* was still functional, did not alter plant growth beyond that observed in *nhx1* or *nhx2* plants and that the importance of NHX3 and NHX4 in plant growth became apparent only in the *nhx1/2* knockout mutant background. The data supported the notion that NHX1 and NHX2 were the main vacuolar NHX antiporters needed for growth and that NHX3 and NHX4 may have additional roles (Bassil et al., 2011b).

The Growth Response to Na^+ and K^+ Depends on Vacuolar NHX Isoforms

The role(s) of some NHX-type antiporters in vacuolar Na^+ and K^+ homeostasis has been discussed previously (Bassil et al., 2012; Bassil and Blumwald, 2014) but is limited mostly to *NHX1* and *NHX2*. To further characterize the cation specificity of all known Arabidopsis vacuolar NHXs and better understand the concerted role that the four antiporter isoforms have on overall vacuolar ion homeostasis, we evaluated the cation-dependent growth of multiple-order vacuolar *NHX*

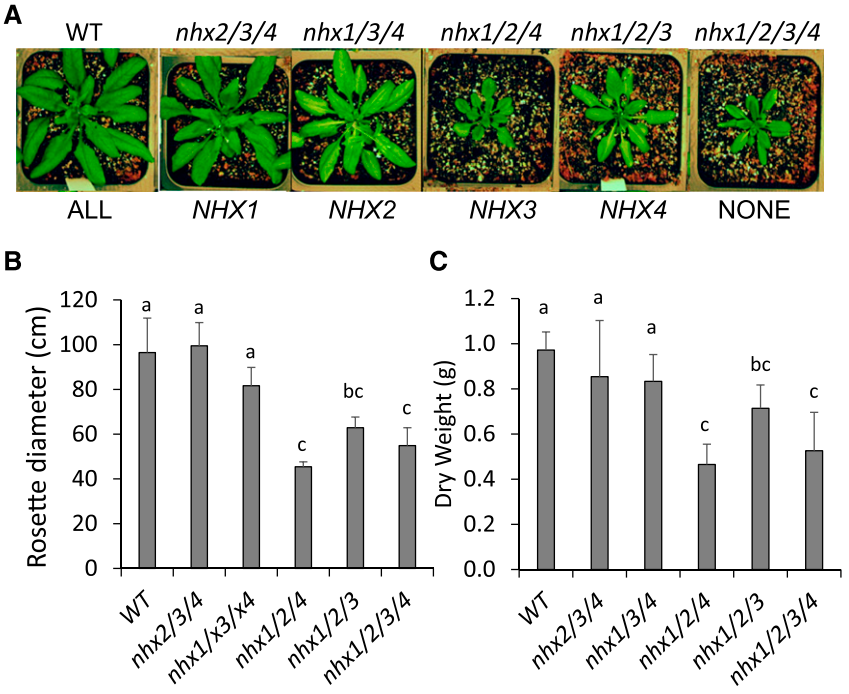

Figure 1. Growth and developmental phenotypes of multiple T-DNA insertion knockout mutants of vacuolar *NHX1*, *NHX2*, *NHX3*, and *NHX4* in Arabidopsis. Multiple-order knockout mutants have either three (*nhx2/3/4*, *nhx1/3/4*, *nhx1/2/4*, and *nhx1/2/3*) or four T-DNA insertions in each of the four vacuolar *NHX*-type cation/H^+ antiporters, as shown above each plant image. The functional copy of the vacuolar *NHX* gene is shown below each image. A, Four-week-old plants grown under 16-h/8-h light/dark at 23°C before flowering. The rosette images were digitally extracted and made into a composite for comparison. B and C, Quantification of rosette diameter (B) and dry weight (C) of whole shoots. Different letters in B and C indicate significant differences using Tukey's LSD test ($P \leq 0.05$). Values are means ± SD ($n = 12$). WT, Wild type.

knockout mutants. Previously, we tested the growth of *nhx1 nhx2* knockouts under different cation concentrations (Bassil et al., 2011b) and concluded that modified Murashige and Skoog (MS) medium supplemented with either 30 mM sodium chloride (NaCl) or 30 mM potassium chloride (KCl) was suitable for growth assays of vacuolar *NHX* knockouts.

We routinely used a modified MS growth medium, prepared according to Spalding et al. (1999) and named SP medium here, rather than the commonly used one-half-strength MS medium (Murashige and Skoog, 1962). In addition to allowing for the precise control of cation and anion concentrations in the medium (Spalding et al., 1999), SP medium represents more physiologically relevant nutrient concentrations as compared with one-half-strength MS medium. When grown in SP medium, the growth of triple and quadruple *NHX* knockout mutants was highly dependent on the presence of either NaCl or KCl in the growth medium (Fig. 2). The wild type showed a 25% decrease in fresh weight in the presence of NaCl but no difference with added KCl (Fig. 2, A, G, M, and S). The growth of *nhx2/3/4* and *nhx1/3/4* plants did not differ from that of the wild type grown in either control medium or medium supplemented with either 30 mM KCl or 30 mM NaCl (Fig. 2, C, I, O, and S). More striking phenotypical differences were seen in triple *NHX* knockout mutants lacking full-length *NHX1* and *NHX2* transcripts (i.e. *nhx1/2/4* and *nhx1/2/3*). In control medium, the knockout mutants *nhx1/2/3* and *nhx1/2/4* and the quadruple knockout mutant *nhx1/2/3/4* all displayed severely reduced growth rates compared with the wild type, similar to that shown in soil-grown plants (Fig. 1). The presence of 30 mM KCl in the growth medium, however, resulted in particularly severe growth reductions in *nhx1/2/4* (40%; Fig. 2, P and S) and *nhx1/2/3* mutant plants (52%; Fig. 2, Q and S) compared with plants grown in control medium. In the *nhx1/2/3/4* quadruple knockout mutants, the addition of KCl to the growth medium induced a reduction in plant growth similar to that noted in *nhx1/2/4* knockout plants (i.e. 40% of control medium). Notably, *nhx1/2/3* knockout mutants were less sensitive than *nhx1/2/4* knockout mutants to added KCl, suggesting a functional difference between NHX4 and NHX3 in mediating K^+ transport and regulating vacuolar K^+ homeostasis. The response to added NaCl was different from that to KCl in all vacuolar knockouts. Added NaCl caused an expected slight reduction in the growth of wild-type, *nhx2/3/4*, and *nhx1/3/4* knockout plants. In *nhx1/2/4* and *nhx1/2/3/4*, growth in the presence of 30 mM NaCl increased rosette fresh

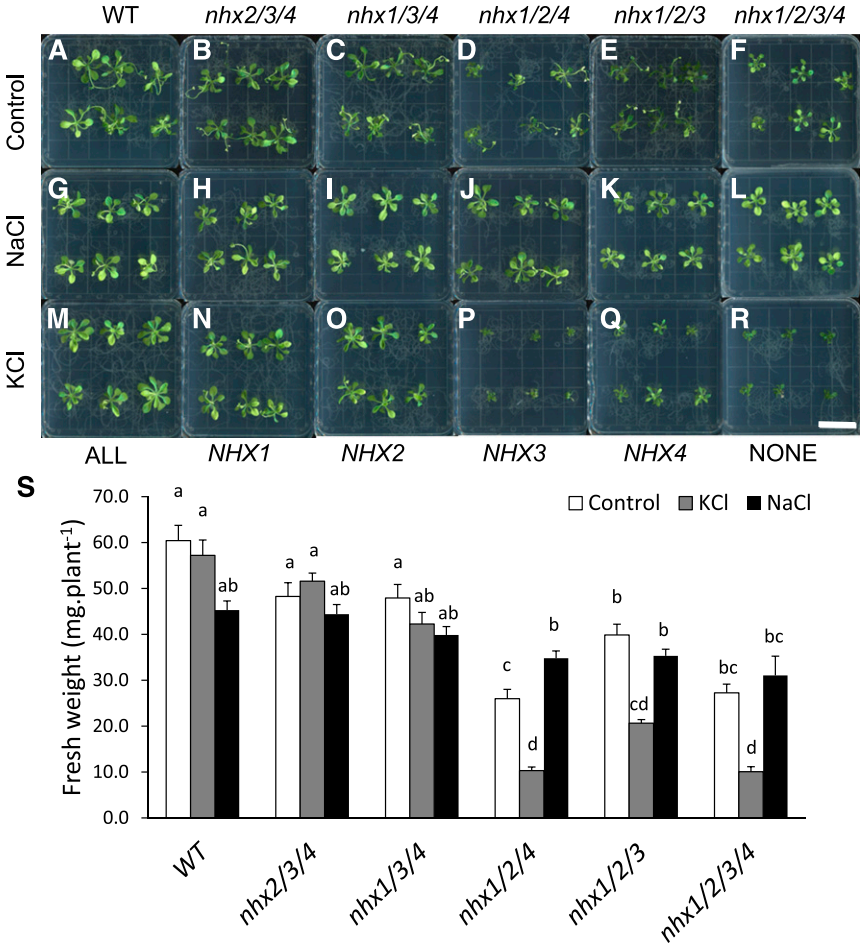

Figure 2. Growth phenotypes of vacuolar *nhx* knockout mutants grown under supplemental NaCl and KCl. Six-day-old wild-type (WT) and knockout mutant plants were transplanted into modified MS medium (SP medium) supplemented with 30 mM NaCl or KCl. A to R, Images of 18-d-old plants. Bar = 2 cm. S, Fresh weights measured after 19 d of growth. Different letters above the bars indicate significant differences using one-way ANOVA with Tukey's LSD separation test ($P \leq 0.05$). Values are means ± SE ($n = 23–40$).

weight by 34% and 14%, respectively. In *nhx1/2/3* plants, added NaCl did not have a significant effect on rosette fresh weight. These results suggested that while both NHX3 and NHX4 mediated Na^+ transport in a similar manner, NHX3 did not transport K^+. The quadruple knockout mutants generated using CRISPR/Cas9-based gene editing (*nhx1/2c/3/4c*) displayed similar phenotypes to corresponding T-DNA insertional mutants (Supplemental Fig. S6). Specifically, the growth of quadruple knockout plants *nhx1/2/3/4* increased by 21% to 37% in the presence of NaCl and decreased by 20% to 33% in the presence of KCl as compared with control medium, similar to what was reported in T-DNA knockouts (Fig. 1). These data supported the notion that the cation-dependent growth responses discussed above were due to the lack of vacuolar NHX and not likely due to pleiotropic effects of T-DNA insertions.

Cation-Dependent Etiolation Responses of Vacuolar NHX Knockouts

Previously, we showed the etiolation response of dark-grown seedlings as a suitable system in which to study cell expansion and useful for the analysis of cellular ion homeostasis (Bassil et al., 2011b). Etiolated seedlings undergo rapid hypocotyl elongation and rely on vacuolar ion uptake to generate the turgor required to drive cell expansion (Gu and Innes, 2012), in which vacuolar NHXs function (Bassil et al., 2011b). We tested the function of each vacuolar *NHX* on both hypocotyl and root elongation using the triple and quadruple *nhx* knockout mutants and asked whether added Na^+ or K^+ altered any etiolation phenotypes similar to longer term growth experiments (Fig. 2). The phenotypes of wild-type and *nhx2/3/4* and *nhx1/3/4* knockout plants were similar in all conditions tested. Marked phenotypical

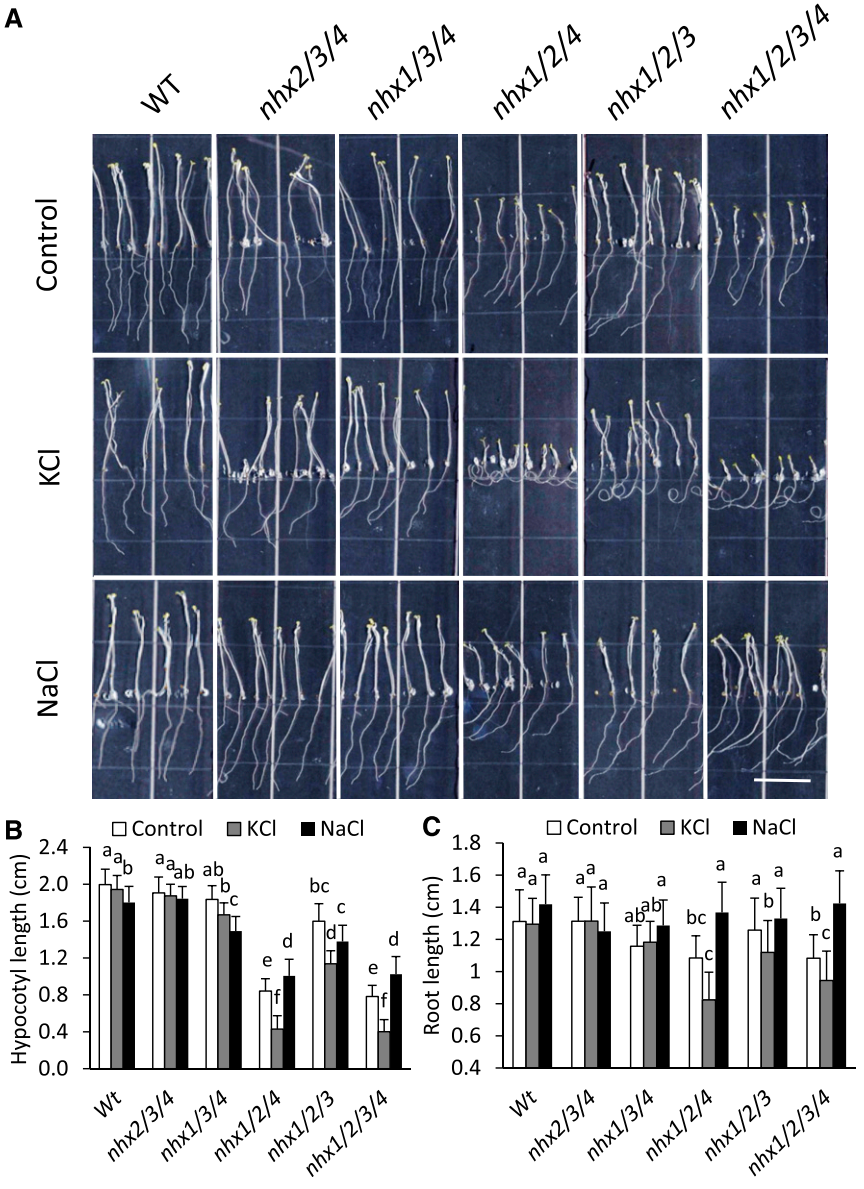

Figure 3. Etiolated seedlings of vacuolar *nhx* knockout mutants grown under supplemental NaCl and KCl. Seedlings were grown on modified MS medium (Spalding et al., 1999) supplemented with 1 mM NaCl and 1 mM KCl (control), 30 mM NaCl, or 30 mM KCl. A, Growth of 11-d-old etiolated seedlings grown in the dark. Bar = 1 cm. B and C, Hypocotyl length (B) and root length (C) measured in the seedlings shown in A. Values are means ± SD (n = 15–25). Different letters above the bars indicate significant differences by one-way ANOVA using Tukey's LSD separation test ($P \leq 0.05$). WT, Wild type.

differences were observed in *nhx1/2/4* and *nhx1/2/3/4* knockout plants in the presence of 30 mM KCl that displayed a clear reduction in hypocotyl length and severe root curling (Fig. 3A). Hypocotyls and roots of *nhx1/2/3* knockout mutants were less affected by KCl than *nhx1/2/4* and *nhx1/2/3/4* (Fig. 3, B and C). The negative effects of KCl on the hypocotyl growth and root curling of *nhx1/2/4* and *nhx1/2/3/4* knockout mutants were not observed when the seedlings were grown in the presence of 30 mM NaCl (Fig. 3), as added NaCl significantly increased both the hypocotyl and root growth of *nhx1/2/4* and *nhx1/2/3/4* knockout mutants compared with growth in the control medium. These results suggest that NHX3 and NHX4 play different roles in maintaining K^+ and Na^+ homeostasis and support the phenotypical growth differences displayed by knockout mutant plants (Fig. 2).

Vacuolar NHX Regulation of Vacuolar Luminal pH

Previous work indicated that NHX1 and NHX2 are important regulators of vacuolar pH (Bassil et al., 2011b). Using live cell imaging and the pH-responsive dye 2′7′-bis-(2-carboxyethyl)-5-(and-6)-carboxyfluorescein-acetoxymethyl ester (BCECF-AM) that rapidly and specifically loads into root cell vacuoles (Krebs et al., 2010; Bassil et al., 2011b), we measured the vacuolar pH in root cells of each triple and quadruple knockout mutant. We also tested the change of vacuolar pH that could occur as a consequence of H^+-coupled vacuolar cation uptake in response to added KCl and NaCl by treating the seedlings with 30 mM KCl or 30 mM NaCl for 1 h prior to pH measurement. pH values were calculated from fluorescence emission ratios of BCECF-AM using an in situ calibration curve (Fig. 4A). Since we were able to quantify the vacuolar pH in individual root cells, we opted to quantify pH in the root tip where vacuolar expansion has not occurred and in the mature zone where cells are highly vacuolated. Vacuolar pH in the root tip cells was more acidic than in comparable mature zone cells, and there was no difference between the wild type and any knockout mutants or salt condition (Fig. 4B). In mature zone cells, the vacuolar pH of both *nhx2/3/4* and *nhx1/3/4* knockout mutants did not differ from those of the wild type in any salt condition (Fig. 4C). However, the vacuolar pH of *nhx1/2/4*, *nhx1/2/3*, and *nhx1/2/3/4* knockout mutants was significantly more acidic (0.2 pH units) than that of the wild type in both control and NaCl-supplemented media. Furthermore, vacuolar pH in roots from *nhx1/2/4* and *nhx1/2/3/4* knockout mutants exposed to KCl was 0.1 pH units more acidic than that of untreated or NaCl-treated seedlings. The difference in vacuolar pH between *nhx1/2/3* and *nhx1/2/4* in untreated or NaCl-treated cells compared with KCl-treated cells supported the notion that NHX3 and NHX4 differed in the control of pH and closely mirrored previous results presented above (Figs. 1 and 2).

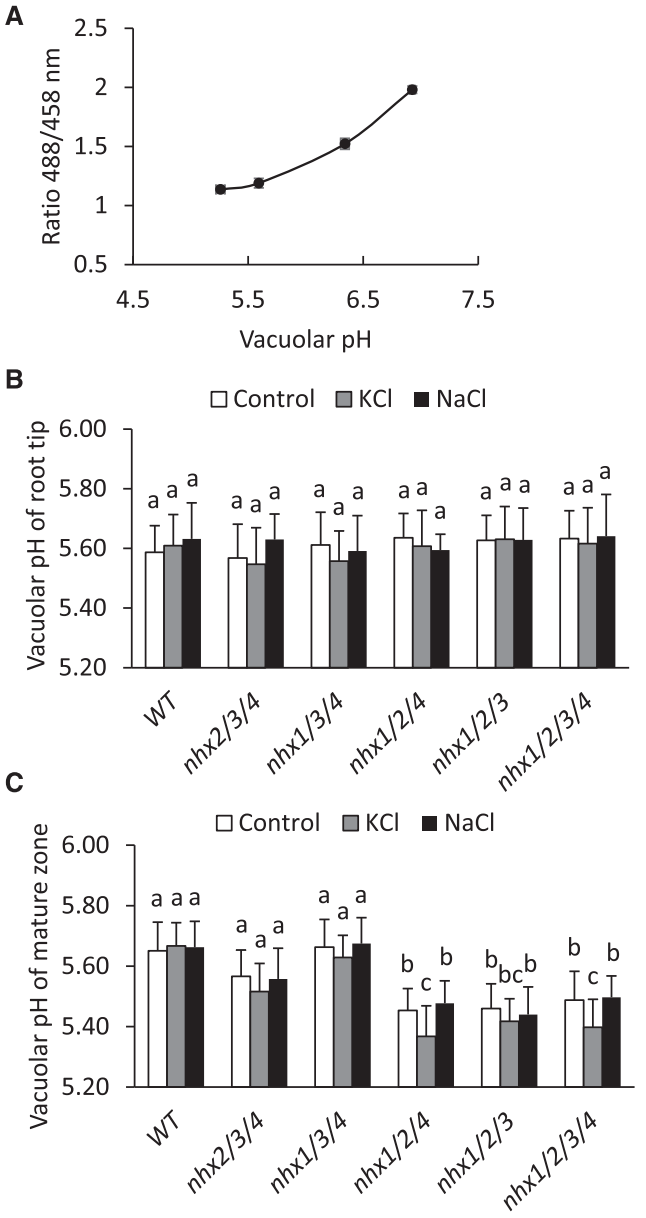

Figure 4. Vacuolar pH in the root tip and mature zone of vacuolar *nhx* knockout mutant roots. Seedlings were sown in SP control medium for 4 d and then transferred to liquid SP medium supplemented with 30 mM KCl, 30 mM NaCl, or no added salt (control) for 1 h. A, Vacuolar pH was measured in roots using the ratiometric dye BCECF-AM following in situ calibration as described in "Materials and Methods." Values are means ± SD ($n = 8$). B and C, Vacuolar pH in the root tip (B) and cells of the mature zone (C). Different letters above the bars indicate significant differences using one-way ANOVA with Tukey's LSD test ($P \leq 0.05$). Values are means ± SD ($n = 24$). WT, Wild type.

Vacuolar Cation Uptake

Given the differential effects of Na^+ and K^+ on triple *nhx* knockout mutant growth and vacuolar pH, we measured vacuolar Na^+ and K^+ transport in knockout mutants. Previously, NHX antiporter transport activities

were quantified from changes in the fluorescence quenching of Acridine Orange-loaded vacuoles and used to measure rates of H^+-coupled cation transport (Blumwald and Poole, 1985; Blumwald et al., 1987; Apse et al., 1999, 2003; see below). To measure vacuolar cation uptake more directly, we developed a fluorescence-based assay using two cation-responsive dyes: Sodium-binding BenzoFuran Isophtalate (SBFI) and Potassium-binding BenzoFuran Isophtalate (PBFI). Both SBFI and PBFI have dual excitation wavelengths near 340 and 380 nm and a single emission wavelength above 505 nm. Because of their ratiometric nature, PBFI and SBFI are better suited for the accurate and reliable quantitation of ion-dependent fluorescence changes than other nonratiometric dyes, such as Sodium Green, CoroNa (Thermo Fisher), or Asante Potassium Green-2 (Teflabs), despite the latter having higher quantum efficiencies and easier loading into plant cells. Ratiometric dyes are less influenced by positional shifts, differences in dye loading, and photobleaching. We opted to use the acetomethoxyl ester (AM) form rather than the acid form of both SBFI and PBFI because the AM conjugation facilitates faster and more consistent loading into vacuoles. The method relies on the continuous measurement of changes in fluorescence emission during cation transport while the vacuoles are under microscopic observation. For the accurate collection of emission measurements, it was necessary to immobilize vacuoles onto microscope slides so that no shifts in position, and therefore emission artifacts, occurred. Vacuoles were effectively immobilized on pretreated slides coated with the negatively charged polymer poly-Asp or poly-Glu (see "Materials and Methods"). We tested the responsiveness of immobilized dye-loaded vacuoles to added NaCl and KCl by generating a standard curve (Fig. 5). Cation-dependent fluorescence changes of SBFI- or PBFI-loaded vacuoles were calibrated against increasing salt (NaCl or KCl) concentrations, and a linear relationship was obtained in the range 0 to 100 mM (Fig. 5B). Representative false-colored images of SBFI- or PBFI-loaded wild-type vacuoles, taken immediately following the addition of either 100 mM NaCl or 100 mM KCl (5 and 500 s later), indicated the changes in fluorescence (Fig. 5A). SBFI-loaded vacuoles did not exhibit a change in fluorescence above background when KCl was added, nor did PBFI-loaded vacuoles in the presence of NaCl. Collectively, these data suggested that the experimental setup allowed for the direct and specific assessment of Na^+- and K^+-dependent vacuolar uptake.

The electrical potential difference across the vacuolar membrane ranges from −10 to −25 mV (the negative sign is given according to the sign convention for endomembranes; Bertl et al., 1992); thus, the transport of K^+ into the vacuole must be active (mediated by H^+-coupled transport) to accumulate K^+ into the vacuole at concentrations above 20 mM (Walker et al., 1996). The uptake of K^+ into the vacuoles displayed saturation kinetics with respect to extravacuolar K^+ concentrations in vacuoles isolated from the wild type and *nhx2/3/4*, *nhx1/3/4*, and *nhx1/2/3* knockout mutants (Fig. 6), with apparent K_m values of 20.3, 25, 26, and 8.5 mM,

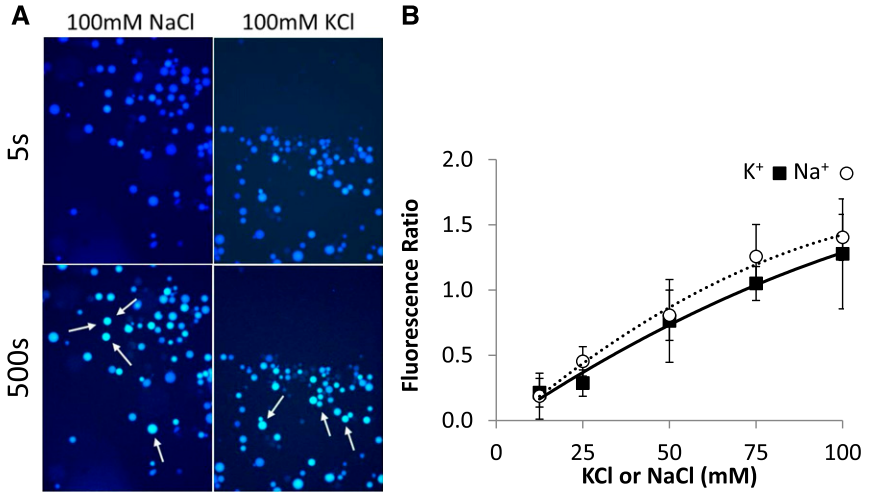

Figure 5. In vivo calibration of K^+- and Na^+-dependent fluorescence in isolated intact leaf vacuoles. Vacuoles from *nhx* T-DNA insertion knockout mutants were loaded with either PBFI-AM (for K^+) or SBFI-AM (for Na^+) in assay buffer and immobilized on coated microscope slides fitted within a chamber. Vacuoles then were incubated with 3 mM Mg-ATP and 50 mM tetramethylammonium chloride (TMA-Cl), and assays were initiated after the addition of varying concentrations of NaCl or KCl and imaged for emission from 500 to 580 nm after sequential excitation with 340 and 380 nm. A, Representative false-colored images at the beginning (5 s) and end (500 s) of a typical transport assay using wild-type vacuoles. Arrows point to individual vacuoles showing a strong increase in fluorescence at the end of the run. B, Fluorescence ratios were calculated after background correction as the difference between starting fluorescence and that at the end of 500 s and plotted against the concentration of added salt to generate the indicated calibration curve. Between 25 and 50 vacuoles of at least three assays at each salt concentration were used to calculate luminal fluorescence and the ratio values for the analysis. Values are means ± SD (n = 3–5).

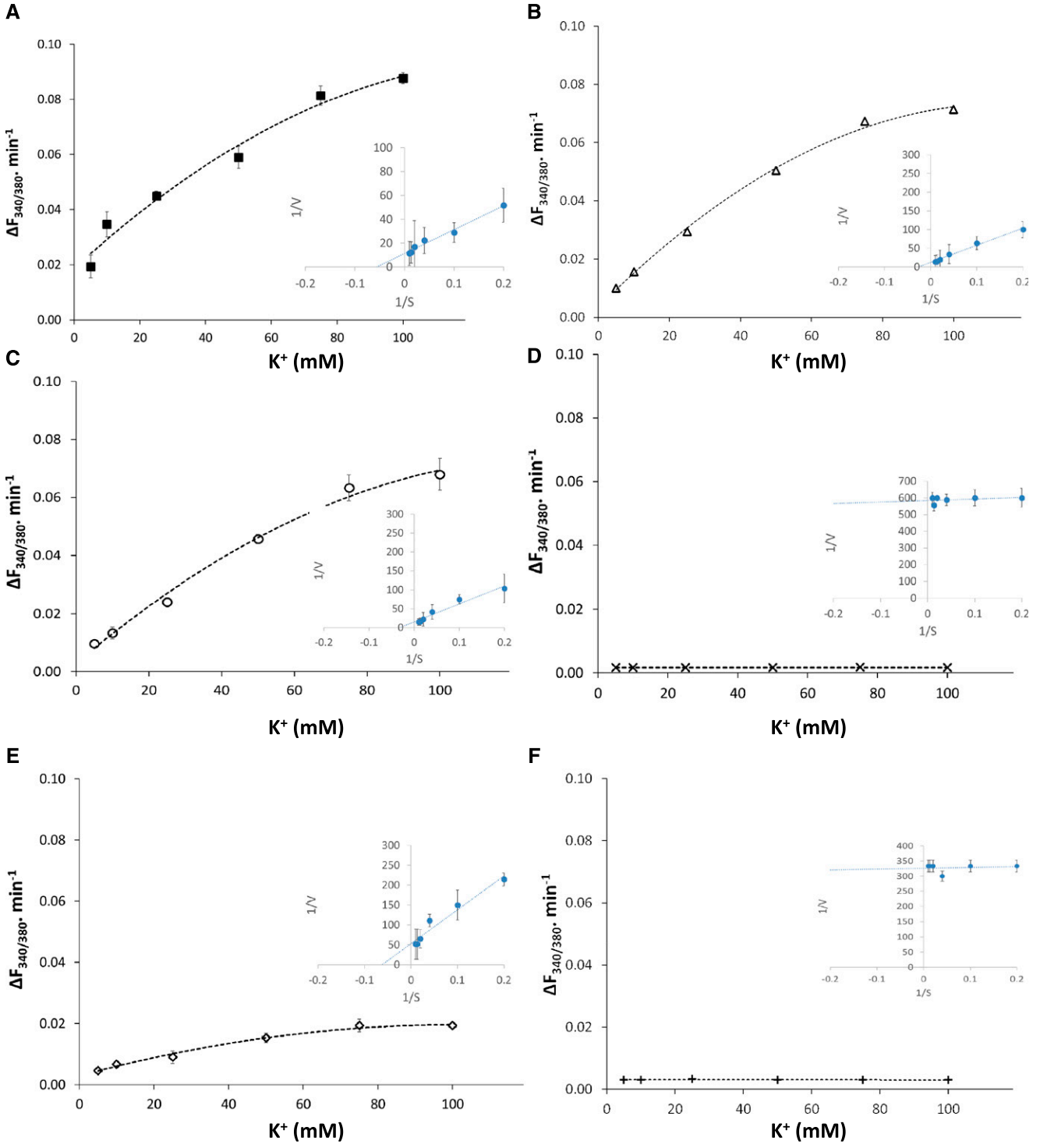

Figure 6. K^+ transport in isolated vacuoles of *nhx* knockout mutant vacuoles. K^+-dependent uptake was calculated from fluorescence changes in PBFI-loaded vacuoles exposed to increasing K^+ concentrations as described in "Materials and Methods" and Figure 4. Values are means ± SD (n = 35–70) of each of three independent experiments. Insets show double-reciprocal plots of K^+-dependent PBFI fluorescence, represented as the change in fluorescence ratio following the addition of KCl. A, The wild type. B, *nhx2/3/4*. C, *nhx1/3/4*. D, *nhx1/2/4*. E, *nhx1/2/3*. F, *nhx1/2/3/4*.

respectively (Fig. 6; Table 1). Interestingly, no K^+ uptake was detected in either *nhx1/2/4* or the quadruple knockout mutant *nhx1/2/3/4* (Fig. 6; Table 1). The uptake of Na^+ into vacuoles from wild-type plants and all the triple knockout mutants displayed saturation kinetics with respect to extravacuolar Na^+ concentrations,

with a comparable apparent K_m of 15.9 to 18.2 mM (Fig. 7; Table 1). Interestingly, the quadruple knockout mutant *nhx1/2/3/4*, lacking functional vacuolar NHX antiporters (NHX1–NHX4), displayed Na^+ transport into the vacuole with a Michaelis-Menten relationship to extravacuolar Na^+, with an apparent K_m of 9.9 mM (Fig. 7; Table 1).

We investigated whether other cation/H^+ exchangers, such as CHXs (Maathuis et al., 2014; Sze and Chanroj, 2018), might play a role in catalyzing Na^+/H^+ exchange by measuring H^+-dependent Na^+ and K^+ transport in vacuoles from the wild type and the quadruple knockout mutant *nhx1/2/3/4* using the fluorescence quenching of Acridine Orange (Blumwald and Poole, 1985; Blumwald et al., 1987; Apse et al., 1999, 2003). Typical traces of vacuolar kinetics from the wild type and the quadruple knockout mutant are shown in Figure 8. The addition of Mg^{2+} and ATP activated the vacuolar V-ATPase, generating an acidic-inside pH gradient (fluorescence quenching). Once steady state was reached, the V-ATPase was inactivated using bafilomycin and the initial rates of H^+-coupled vacuolar cation transport were measured by monitoring the recovery of fluorescence upon the addition of NaCl or KCl (Fig. 8). Wild-type vacuoles displayed a K^+- or Na^+-dependent fluorescence recovery (indicative of cation-coupled H^+ transport), while no significant fluorescence recovery was seen upon the addition of Na^+ or K^+ to acidified vacuoles from *nhx1/2/3/4* knockout mutants (Fig. 8; Table 2). The more pronounced acidification, upon activation of the V-ATPase, in the vacuoles from the quadruple knockout mutant was likely a consequence of the lack of H^+-coupled cation transporters and the concomitant absence of H^+ leaks that could reduce the electrochemical proton gradients generated by the action of the vacuolar H^+ pump.

DISCUSSION

Vacuolar NHXs and Plant Growth

Using a reverse genetic approach, we characterized the function of all four *NHX* vacuole-localized antiporters. Triple knockout mutants lacking all but one of the four vacuolar NHX isoforms present in Arabidopsis allowed us to assess the ion transport activities of each NHX isoform and their contribution to vacuolar homeostasis and to plant growth. We also generated a quadruple knockout mutant lacking all four vacuolar NHXs using both available T-DNA insertion knockouts and CRISPR/Cas9 gene editing. Without multiple-order knockout mutants, it would be difficult to assess the function of individual vacuolar NHXs in planta.

The growth phenotypes of all triple and quadruple NHX knockout mutants suggested that AtNHX1 and AtNHX2 are the main vacuolar NHX-type antiporters and that these are at least partially redundant (Bassil et al., 2011b; Barragán et al., 2012). This was concluded from the fact that the triple knockout mutants *nhx2/3/4* and *nhx1/3/4*, in which either *NHX1* or *NHX2* is expressed, displayed phenotypes similar to the wild type. Lack of NHX3 and NHX4 did not significantly affect shoot biomass if either *NHX1* or *NHX2* was expressed, suggesting that NHX3 and NHX4 are minor contributors to Arabidopsis growth. In *nhx3* and *nhx4* single knockout mutants, plant growth is not affected significantly (Li et al., 2009; Liu et al., 2010); however, in knockouts lacking both NHX1 and NHX2 and either NHX3 and NHX4 (i.e. *nhx1/2/3* or *nhx1/2/4*), growth was more severely compromised than in *nhx1/2* double knockouts (Bassil et al., 2011b; Barragán et al., 2012). These data suggested complex interactions between the four vacuolar NHXs in Arabidopsis.

Publicly available vacuolar *NHX* gene expression data (Schmid et al., 2005; Waese et al., 2017) and previous results from our group (Bassil et al., 2011b) indicate that *NHX1* is the strongest expressed vacuolar *NHX* in Arabidopsis, followed by *NHX2*, whereas the expression of *NHX3* and *NHX4* is only approximately one-tenth of the expression level of *NHX1*, except in guard cells and the vasculature, where *NHX3* and *NHX4* transcripts are more abundant. It is possible that NHX3 and NHX4 fulfill more important functions under conditions or in tissues where NHX1 and NHX2 are not dominant. Furthermore, the close similarity in growth, at least under the conditions described here, between the *nhx1/2/4* and *nhx1/2/3/4* knockout mutants suggests a secondary importance of NHX3.

The NHX knockout mutants *nhx1/2/3*, *nhx1/2/4*, and *nhx1/2/3/4* displayed striking phenotypical responses to exogenous KCl and NaCl. Both root and shoot growth was strongly stunted in the presence of 30 mM KCl, while it was stimulated by 30 mM NaCl. The high sensitivity to added K^+ was likely a consequence of the aberrant K^+ accumulation in the cytosol, as suggested from previous results in the double knockout mutant *nhx1/2* (Bassil et al., 2011b; Barragán et al., 2012). At typical plasma membrane and tonoplast electrical potential differences of −120 mV and approximately+30 mV, respectively, K^+ uptake into the cell would be passive but require active transport to accumulate into the vacuole above approximately20 mM (Martinoia

Table 1. *Apparent K_m for K^+ and Na^+ transport in vacuoles isolated from the wild type and* nhx *knockout mutants*

The apparent K_m values were calculated by the intersection of the fitted line with the abscissa of the double reciprocal plots for the K^+-dependent PBFI fluorescence changes (Fig. 6, insets) and the Na^+-dependent SBFI fluorescence changes (Fig. 7, insets). Values are means ± SD (n = 6).

Plant	K^+	Na^+
Wild type	20.3 ± 2.4	17.6 ± 3.4
(*NHX1*) *nhx2/3/4*	25 ± 5.3	17.1 ± 5.5
(*NHX2*) *nhx1/3/4*	26 ± 3.4	18.2 ± 1.9
(*NHX3*) *nhx1/2/4*	0	15.3 ± 6.4
(*NHX4*) *nhx1/2/3*	8.5 ± 3.5	15.8 ± 1.9
(None) *nhx1/2/3/4*	0	9.9 ± 0.2

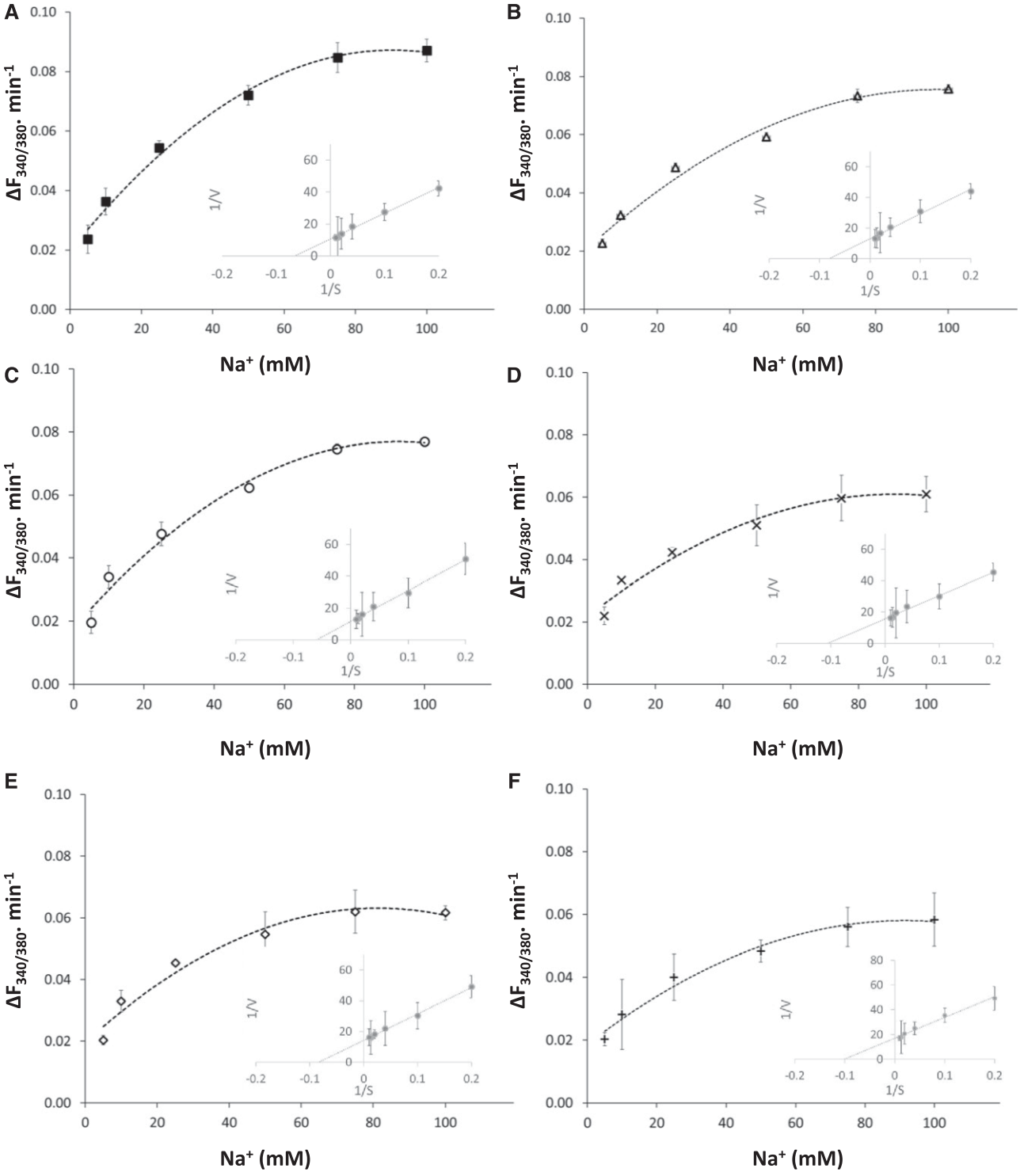

Figure 7. Na^+ transport in isolated vacuoles of *nhx* knockout mutant vacuoles. Na^+-dependent uptake was calculated from fluorescence changes in SBFI-loaded vacuoles exposed to increasing Na^+ concentrations as described in "Materials and Methods" and Figure 4. Values are means ± SD (n = 35–70) of each of three independent experiments. Insets show double-reciprocal plots of Na^+-dependent SBFI fluorescence, represented as the change in fluorescence ratio following the addition of NaCl. A, The wild type. B, *nhx2/3/4*. C, *nhx1/3/4*. D, *nhx1/2/4*. E, *nhx1/2/3*. F, *nhx1/2/3/4*.

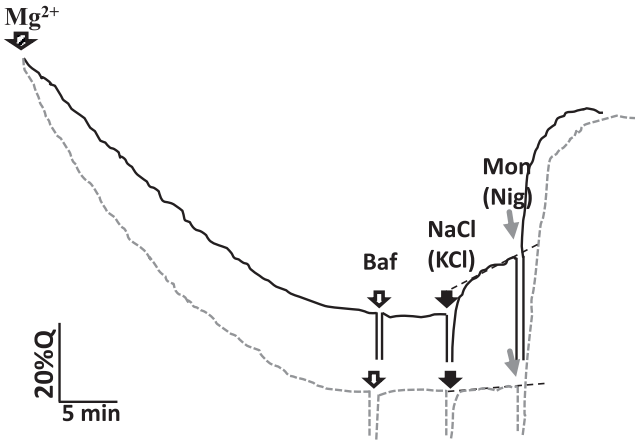

Figure 8. Cation-dependent H^+ antiport activity in isolated leaf vacuoles. Fluorescence quenching of Acridine Orange was used to monitor the dissipation of inside-acid pH changes in vacuoles (see "Materials and Methods"). The addition of Mg^{2+} initiated H^+ translocation and fluorescence change (quenching) of Acridine Orange until a steady-state gradient was formed. Ten nanomolar bafilomycin (Baf) was added to stop vacuolar H^+-ATPase H^+ translocation. Following a constant rate of fluorescence, aliquots of NaCl or KCl were added and changes in fluorescence recovery were determined (initial rates). The addition of either nigericin (Nig) or monensin (Mon), the artificial K^+/H^+ or Na^+/H^+ antiporter, respectively, was used to abolish the pH gradient and recover fluorescence fully. Shown are typical traces from the wild type (solid line) and the quadruple T-DNA insertion knockout mutant *nhx1/2/3/4* (dotted line). Gaps in the recording result from the addition of the indicated reagents. Q, Percentage of fluorescence quenching.

et al., 2000; Leigh, 2001; Wang and Wu, 2013). Therefore, the lack of NHX-mediated transport at the tonoplast, even at the relatively low external K^+ concentration of 30 mM, could lead to an aberrant accumulation of K^+ in the cytosol that would be deleterious to the cell and result in the strong growth phenotypes reported here. The difference in sensitivity to added K^+ between *nhx1/2/3* and *nhx1/2/4* knockout mutants (the latter being more sensitive than the former; Fig. 2) suggested that, in Arabidopsis, NHX4 is more important for vacuolar K^+ uptake than is NHX3.

Interestingly, Arabidopsis seedling roots of triple knockouts lacking *NHX1*, *NHX2*, *NHX3*, and/or *NHX4* also displayed strong curling and a loss of directional growth under added KCl. The curling phenotype could be a consequence of uneven cell expansion but also could result from the disorganization of the cytoskeleton from direct or indirect effects of high cytosolic K^+ (McCubbin et al., 2014). Further investigation is needed to assess the relationship between intracellular ion homeostasis and cytoskeleton dynamics and reorganization in these plants.

Table 2. *Cation-dependent H^+ antiporter activity in isolated leaf vacuoles*

Initial rates of cation-dependent H^+ transport (Fig. 8) are shown. %Q, Percentage of fluorescence quenching.

Plant	100 mM NaCl	100 mM KCl
	%Q min^{-1}	
Wild type	2.02 ± 0.38	1.98 ± 0.27
nhx1/2/3/4	0.09 ± 0.08	0.10 ± 0.10

Transport Kinetics of Vacuolar NHXs

Previously, we used the ratiometric K^+-binding dye PBFI-AM to investigate the role of NHX1 and NHX2 in mediating vacuolar K^+ uptake (Bassil et al., 2011b). We found that the steady-state concentration of K^+ in Columbia-0 wild-type root and hypocotyl cell vacuoles was approximately 75 mM, while in double knockout mutant *nhx1/2* cells, the vacuolar K^+ concentration was 30 mM (Bassil et al., 2011b). Barragán et al. (2012) used energy-dispersive x-ray spectroscopy to estimate vacuolar K^+ pools of leaf mesophyll cells and reported lower counts associated with K^+. The same authors also reported higher cytosolic K^+ activity in root cells impaled with microelectrodes. Although all these techniques allowed for the measurement of steady-state cellular K^+ concentrations, these methods cannot be used reliably to measure vacuolar K^+ uptake kinetics. Here, we opted for the use of isolated vacuoles, rather than intact tissue, to have direct access to tonoplast kinetics without the hindrance of multiple cellular compartments. It was also imperative to immobilize the vacuoles during transport assays to measure changes in fluorescence that correlated with ion uptake into the vacuoles without positional shifts of dye-loaded vacuoles. Unlike the commonly used, positively charged poly-L-Lys, the use of poly-Asp or poly-Glu was more effective at maintaining the vacuoles in place during perfusion and washing. Using this experimental system, we were able to measure K^+ and Na^+ accumulation and associated uptake kinetics in intact vacuoles isolated from the different knockout plants.

Potassium is an important cofactor for charge balance, biosynthesis, and enzymatic activity in the cytosol (Bassil and Blumwald, 2014). Cellular K^+ homeostasis is accomplished through the uptake of extracellular K^+ (Britto and Kronzucker, 2008) and the efflux of K^+ from vacuolar pools (Gierth and Mäser, 2007). K^+ uptake at the plasma membrane is mediated by high-affinity H^+-coupled transporters (HAKs and CHXs; Epstein et al., 1963; Gierth and Mäser, 2007; Sze and Chanroj, 2018) driven by the proton-motive force generated by the plasma membrane-bound H^+-ATPase and by low-affinity K^+ channel transport systems (AKTs and KATs; Maathuis and Sanders, 1995; Wang and Wu, 2013) driven by the negative electrical potential of the plasma membrane (150–180 mV). K^+ release from the vacuoles can be mediated by the action of tonoplast channels: fast- and slow-activating nonselective cation channels and a K^+-selective (two-pore potassium) channel (Wang and Wu, 2013, and refs. therein). K^+ transport into vacuoles is active and mediated by H^+-coupled transporters (Bassil and Blumwald, 2014).

Although a number of H^+-coupled K^+ transporters have been identified in plants, such as HAK/KUP (Gierth and Mäser, 2007) and CHXs (Sze and Chanroj, 2018), only NHXs have been localized to the vacuole (McCubbin et al., 2014). Vacuolar ion transport kinetics, including estimates of apparent K_m for K^+ and Na^+, indicated that K^+ transport was evident in vacuoles expressing Arabidopsis *NHX1*, *NHX2*, and *NHX4*, suggesting that these are the main transporters mediating vacuolar K^+ uptake. NHX3 did not mediate any significant K^+ transport. This was supported by the very poor growth of plants expressing only *NHX3* with K^+ in the growing medium, whereas plants expressing only *NHX4* were less affected by similar K^+ supply. Differences in cation selectivity between NHX3 and NHX4 could be related to specific amino acid residues in putative cation translocation sites, as predicted by a partial sequence alignment (Supplemental Fig. S7).

Values for vacuolar pH in *nhx* knockout mutants related well with cation-dependent growth and were indicative of vacuolar cation/H^+ exchange. For example, although the vacuolar pH in the knockout mutants *nhx1/2/4*, *nhx1/2/3*, and *nhx1/2/3/4* was overall significantly more acidic than that in the wild type and other knockout mutants in which either *NHX1* or *NHX2* was expressed, the knockout mutant expressing only *NHX3* had a significantly lower pH in the presence of KCl in the growth medium, consistent with the notion that NHX3 is not involved in K^+/H^+ exchange.

The affinity of the vacuolar NHX cation/H^+ exchange activity for K^+ and Na^+ has been determined in intact vacuoles (Blumwald et al., 1987; Apse et al., 1999) and tonoplast vesicles (Blumwald and Poole, 1985; Barkla et al., 1995; Hanana et al., 2007) from different plant species and in AtNHX1 reconstituted into lipid vesicles (Venema et al., 2002). In all cases, the reaction displayed saturation kinetics with increasing cation concentrations, with apparent K_m values for Na^+ and K^+ in the range of 10 to 40 mM, indicating that the vacuolar NHX antiporters have a low affinity for Na^+ and K^+. Vacuolar Na^+ uptake was observed in all vacuolar NHX knockout mutants, albeit at different rates. Apparent K_m values for Na^+ in all four triple knockout mutants were in the range of those reported previously and were significantly higher than that of the quadruple knockout mutant, suggesting that all vacuolar NHXs mediate Na^+ transport (Table 1).

The immobilization of intact vacuoles onto pretreated microscope slides enabled loading of the vacuoles with the ratiometric fluorescent dyes SBFI and PBFI. Because of the minimal background dye interference, it was possible to calibrate the cation-dependent dye fluorescence emission and measure pH-dependent cation movements into the acidic vacuoles. Although the method enabled the measurement of the apparent affinity (K_m) of each NHX isoform to Na^+ and K^+, our measurements were not suitable for the calculation of maximal rates of transport (V_{max}). This limitation is due to the variable size of the vacuoles in each preparation; as a consequence, differences in the surface area-to-volume ratio of the vacuoles change the number of NHX proteins mediating the cation transport and concomitantly the cation fluxes. Furthermore, the poor accuracy of the measurement of individual vacuole size prevented a meaningful normalization of data based on this criterion.

Notably, Na^+ uptake into *nhx1/2/3/4* mutant vacuoles indicated that another NHX-independent transport pathway likely exists in Arabidopsis vacuoles. The absence of cation-dependent H^+ transport in the vacuoles from the *nhx1/2/3/4* quadruple knockout mutant would suggest that such vacuolar Na^+ uptake was not H^+ coupled (Fig. 8), which would exclude many of the already known CHX-type cation/H^+ exchangers that could fulfill such a role (Sze and Chanroj, 2018). Out of the few remaining candidate transporters that could mediate Na^+ uptake into the vacuole (Martinoia et al., 2012; Eisenach et al., 2015), an Na^+ channel is not likely, since Na^+ transport into vacuoles would be against its electrochemical potential and would require energization or coupling to H^+. A possible candidate could be an Na^+/Ca^{2+} transporter, but so far, the only vacuole-localized Na^+-coupled transporter (other than NHXs or CHXs) is an Arabidopsis Na^+/Ca^{2+} exchanger (NCL) that mediates Na^+ uptake in exchange for Ca^{2+} efflux into the cytosol (Li et al., 2016). Clearly, the identification of the vacuolar H^+-independent Na^+ transporter requires more investigation.

In summary, we showed that, in Arabidopsis, tonoplast-localized NHX1, NHX2, and NHX4 are the main transporters involved in the uptake of K^+ into vacuoles. NHX4 may have a high affinity for K^+ and is less significant in Na^+ uptake. Our data also suggest that NHX3 is involved in vacuolar Na^+ transport, as evidenced by transport kinetics as well as the growth responses of vacuolar *NHX* knockout mutants. Because Na^+ uptake into vacuoles was measured in the quadruple *nhx* knockout lacking any NHX antiport activity and was not H^+ coupled, we conclude that another H^+-independent Na^+ conductive pathway likely exists in Arabidopsis vacuoles. Importantly, these data corroborate the large body of experimental evidence that demonstrates the role of NHX-type cation/H^+ exchangers in vacuolar Na^+ uptake.

MATERIALS AND METHODS

Plant Materials

All Arabidopsis (*Arabidopsis thaliana*) T-DNA insertion mutants were in the Columbia-0 ecotype and were obtained from http://signal.salk.edu/cgi-bin/tdnaexpress. Mutant alleles and the corresponding T-DNA insertion lines are shown in Supplemental Figure S1 and were designed as follows: *NHX1* (At5g27150) are *nhx1-1* (SALK_034001) and *nhx1-2* (SALK_065623); *NHX2* (At3g05030) are *nhx2-1* (SALK_036114) and *nhx2-3* (SALK_084844); *NHX3* (At5g55470) are *nhx3-1* (WiscDsLox345-348F19) and *nhx3-2* (SALK_082277); *NHX4* (At3g06370) are *nhx4-1* (SALK_112901) and *nhx4-2* (GABI_654D09). The selection of insertion knockouts with homozygous T-DNA insertion was confirmed by genomic PCR, resulting in both the absence of PCR amplification with two allele-specific primers corresponding to 5′ and 3′ sides of the T-DNA insertion and the presence of PCR amplification with one allele-specific primer and a T-DNA primer corresponding to the left border. Genomic PCR was

performed twice with independently isolated genomic DNA. Reverse transcription PCR confirmed no DNA amplification with allele-specific primers from knockout-derived cDNA. Allele-specific primers are shown in Supplemental Table S1. Plants were grown in soil at 22°C under 16 h of light (Bassil et al., 2011b).

Generation of Alternative Quadruple Knockout Mutants Using CRISPR/Cas9

The CRISPR/Cas9 construct targeting *NHX2* and *NHX4* was generated in pYLCRISPR/Cas9Pubi-H vector (Ma et al., 2015). The primers and the template DNA used for the first and second PCR are listed in Supplemental Tables S2 and S3. Each PCR was performed in 12 μL using CloneAmp HiFi PCR premix (Takara Bio) for 28 cycles (98°C for 10 s, 55°C for 5 s, and 72°C for 10 s). Second PCR products were pooled and purified using NucleoSpin Gel and PCR Clean-Up (Takara Bio). Golden Gate assembly was performed in 1× CutSmart buffer (New England Biolabs), 1× T4 DNA ligase buffer (New England Biolabs), 10 units of *Bsa*I-HF (New England Biolabs), 40 units of T4 DNA ligase (New England Biolabs), 100 ng of pooled sgRNA cassettes, and 100 ng of pYLCRISPR/Cas9Pubi-H. The reactions were incubated in a thermal cycler for three cycles (37°C for 10 min, 10°C for 5 min, and 20°C for 5 min) followed by 10 cycles (37°C for 3 min, 10°C for 5 min, and 20°C for 5 min). The ligated products were used directly for transformation in TOP10 competent cells (Invitrogen). Positive colonies were verified by sequencing and *Mlu*I digestion. The construct was delivered by *Agrobacterium tumefaciens* (GV3101) using floral dipping (Clough and Bent, 1998) of *nhx1-2/3-2* plants.

Growth of Mutants in Na^+- and K^+-Supplemented Media

Seeds were surface sterilized, vernalized for 3 d at 4°C, sown on control plates, and grown vertically to facilitate damage-free transfer to treatment plates. Six-day-old plants were transplanted into modified MS medium prepared according to Spalding et al. (1999), containing 0.8% (w/v) Suc, 2.5 mM MES, pH 5.7, and 0.8% (w/v) phytagel with 30 mM NaCl or 30 mM KCl. The fresh weight of whole seedlings was assessed after 19 d of growth in 12 h/12 h of light/dark at 22°C.

RNA Preparation and Expression Analysis

For RT-qPCR, total RNA was treated with DNaseI and purified subsequently with an RNeasy RNA purification column (Qiagen). First-strand cDNA was synthesized from 2.5 mg of the column-purified total RNA with oligo(dT)20 primers using SuperScript II (Invitrogen) and diluted with 10× volume of water. RT-qPCR was performed with cDNA prepared from alleles of *nhx* mutants to confirm the lack of or reduced amplification of PCR products. Control cDNA was prepared from wild-type plants. The same tissues were used for the total RNA preparation from both the wild type and mutants. Allele-specific primers are listed in Supplemental Table S1. RT-qPCR was performed in a duplicate 25-mL reaction mixture containing 5 mL of diluted cDNA solution, 12.5 mL of iQ SYBR Green Supermix (Bio-Rad), and 0.5 mL of each primer (final concentration of 200 nM). PCR was initiated with denaturation at 95°C for 3 min, followed by 40 cycles of denaturation at 95°C for 30 s, annealing at 60°C for 30 s, and extension at 72°C for 30 s. The comparative threshold cycle method was used to determine the relative mRNA levels. *ACT2* or *UBI5* was used as an internal reference, and transcript levels are presented as relative values to the control treatment.

Measurement of Vacuolar pH

pH was measured using the pH-responsive dye BCECF-AM (Thermo Fisher) as described previously (Bassil et al., 2011b).

Vacuole Isolation and in Vivo Perfusion Assays

Intact vacuoles were extracted as described previously (Apse et al., 1999, 2003) from leaves of 3-week-old plants grown in soil (Bassil et al., 2011b). Vacuoles were loaded with 2 μM either K^+-binding PBFI-AM or Na^+-binding SBFI-AM dye (Thermo Fisher) in assay buffer containing 0.4 M mannitol and 5 mM Tris/MES, pH 8, for 1 h and allowed to stick for 30 min to poly-Asp-coated microscope slides (0.1 mg mL^{-1}) fitted within a custom-made perfusion chamber. Vacuoles were incubated with 3 mM Mg-ATP and 50 mM TMA-Cl for 3 min and subsequently exposed to different concentrations of NaCl or KCl. The perfusion flow rate was adjusted to 0.8 mL min^{-1}, and the chamber volume was 0.2 mL. Beginning immediately after salt addition, vacuoles were imaged for emission from 500 to 580 nm after sequential excitation with 340 and 380 nm by capturing frames every 5 s for 500 s. Ratio imaging was performed on a Leica DMRE epifluorescence microscope fitted with a 40× air objective, a Sutter Instruments filter wheel, and a Lambda controller and running the MEtaFluor/MetaMorph (Molecular Devices) software package (version 7.1). In situ calibration of isolated intact vacuoles using known concentrations of KCl and NaCl was performed at the end of each experiment. At the end of each experiment, 2 μM gramicidin D and either 2 μM monensin (Na^+) or nigericin (K^+) were added to equilibrate the salt with the incubation medium and to recover fluorescence. Luminal vacuolar fluorescence was corrected for background before the calculation of ratio values. Between 25 and 50 vacuoles in each of six to 10 independent assays were measured for each salt concentration.

Cation-Dependent H^+ Transport

The fluorescence quenching of Acridine Orange was used to measure Na^+- or K^+-dependent H^+ antiporter activity as described before (Blumwald et al., 1987; Apse et al., 1999). Vacuoles (1×10^4) were added to 0.8 mL of buffer containing 0.4 M mannitol, 1 mM DTT, 25 mM TMA-Cl, 3 mM Tris-ATP, 5 μM Acridine Orange, and 10 mM Tris-MES, pH 8. Proton translocation was initiated by the addition of 3 mM $MgSO_4$, and the change in fluorescence with time was measured as described before (Blumwald et al., 1987).

Accession Numbers

Sequence data from this article can be found in the Arabidopsis TAIR database under the following accession numbers: *AtNHX1*, At5g27150; *AtNHX2*, At3g05030; *AtNHX3*, At5g55470; and *AtNHX4*, At3g06370.

Supplemental Data

The following supplemental materials are available.

Supplemental Figure S1. T-DNA insertion lines used to generate knockout mutant plants.

Supplemental Figure S2. Crossing strategy used to generate multiple knockout mutants of vacuolar *NHXs*.

Supplemental Figure S3. RT-qPCR of *NHX* expression in vacuolar *nhx* knockout mutants.

Supplemental Figure S4. Strategy used to create CRISPR/Cas9 vacuolar *nhx* knockout mutants.

Supplemental Figure S5. Selection of CRISPR/Cas9 vacuolar *nhx* knockout mutants.

Supplemental Figure S6. Growth responses of CRISPR/Cas9 *nhx* knockout mutants in Na^+ and K^+.

Supplemental Figure S7. Amino acid sequence alignment of vacuolar NHXs.

Supplemental Table S1. List of primers used in this study.

Supplemental Table S2. List of primers used in this study for CRISPR/Cas9.

Supplemental Table S3. DNA templates used for CRISPR/Cas9.

ACKNOWLEDGMENTS

We thank the Salk Institute Genomic Analysis Laboratory for generating the sequence-indexed Arabidopsis T-DNA insertion mutants and the Arabidopsis Biological Resource Center for providing them.

Received September 6, 2018; accepted November 7, 2018; published November 29, 2018.

LITERATURE CITED

Amtmann A, Leigh R (2010) Ion homeostasis. *In* A Pareek, SK Sopory, HJ Bohnert, eds, Abiotic Stress Adaptation in Plants. Springer, Dordrecht, The Netherlands, pp 245–262

Andrés Z, Pérez-Hormaeche J, Leidi EO, Schlücking K, Steinhorst L, McLachlan DH, Schumacher K, Hetherington AM, Kudla J, Cubero B, et al (2014) Control of vacuolar dynamics and regulation of stomatal aperture by tonoplast potassium uptake. Proc Natl Acad Sci USA **111:** E1806–E1814

Apse MP, Aharon GS, Snedden WA, Blumwald E (1999) Salt tolerance conferred by overexpression of a vacuolar Na^+/H^+ antiport in Arabidopsis. Science **285:** 1256–1258

Apse MP, Sottosanto JB, Blumwald E (2003) Vacuolar cation/H^+ exchange, ion homeostasis, and leaf development are altered in a T-DNA insertional mutant of AtNHX1, the Arabidopsis vacuolar Na^+/H^+ antiporter. Plant J **36:** 229–239

Barkla BJ, Zingarelli L, Blumwald E, Smith J (1995) Tonoplast NA^+/H^+ antiport activity and its energization by the vacuolar H^+-ATPase in the halophytic plant *Mesembryanthemum crystallinum* L. Plant Physiol **109:** 549–556

Barragán V, Leidi EO, Andrés Z, Rubio L, De Luca A, Fernández JA, Cubero B, Pardo JM (2012) Ion exchangers NHX1 and NHX2 mediate active potassium uptake into vacuoles to regulate cell turgor and stomatal function in Arabidopsis. Plant Cell **24:** 1127–1142

Bassil E, Blumwald E (2014) The ins and outs of intracellular ion homeostasis: NHX-type cation/H^+ transporters. Curr Opin Plant Biol **22:** 1–6

Bassil E, Ohto MA, Esumi T, Tajima H, Zhu Z, Cagnac O, Belmonte M, Peleg Z, Yamaguchi T, Blumwald E (2011a) The Arabidopsis intracellular Na^+/H^+ antiporters NHX5 and NHX6 are endosome associated and necessary for plant growth and development. Plant Cell **23:** 224–239

Bassil E, Tajima H, Liang YC, Ohto MA, Ushijima K, Nakano R, Esumi T, Coku A, Belmonte M, Blumwald E (2011b) The Arabidopsis Na^+/H^+ antiporters NHX1 and NHX2 control vacuolar pH and K^+ homeostasis to regulate growth, flower development, and reproduction. Plant Cell **23:** 3482–3497

Bassil E, Coku A, Blumwald E (2012) Cellular ion homeostasis: Emerging roles of intracellular NHX Na^+/H^+ antiporters in plant growth and development. J Exp Bot **63:** 5727–5740

Bertl A, Blumwald E, Coronado R, Eisenberg R, Findlay G, Gradmann D, Hille B, Köhler K, Kolb HA, MacRobbie E, et al (1992) Electrical measurements on endomembranes. Science **258:** 873–874

Blumwald E, Poole RJ (1985) Na/H antiport in isolated tonoplast vesicles from storage tissue of *Beta vulgaris*. Plant Physiol **78:** 163–167

Blumwald E, Rea PA, Poole RJ (1987) Preparation of tonoplast vesicles: Applications to H^+-coupled secondary transport in plant vacuoles. Methods Enzymol **148:** 115–123

Britto DT, Kronzucker HJ (2008) Cellular mechanisms of potassium transport in plants. Physiol Plant **133:** 637–650

Chanroj S, Wang G, Venema K, Zhang MW, Delwiche CF, Sze H (2012) Conserved and diversified gene families of monovalent cation/H^+ antiporters from algae to flowering plants. Front Plant Sci **3:** 25

Clough SJ, Bent AF (1998) Floral dip: A simplified method for Agrobacterium-mediated transformation of *Arabidopsis thaliana*. Plant J **16:** 735–743

Eisenach C, Francisco R, Martinoia E (2015) Plant vacuoles. Curr Biol **25:** R136–R137

Epstein E, Rains DW, Elzam OE (1963) Resolution of dual mechanisms of potassium absorption by barley roots. Proc Natl Acad Sci USA **49:** 684–692

Gierth M, Mäser P (2007) Potassium transporters in plants: Involvement in K^+ acquisition, redistribution and homeostasis. FEBS Lett **581:** 2348–2356

Gu Y, Innes RW (2012) The KEEP ON GOING protein of *Arabidopsis* regulates intracellular protein trafficking and is degraded during fungal infection. Plant Cell **24:** 4717–4730

Hanana M, Cagnac O, Yamaguchi T, Hamdi S, Ghorbel A, Blumwald E (2007) A grape berry (Vitis vinifera L.) cation/proton antiporter is associated with berry ripening. Plant Cell Physiol **48:** 804–811

Krebs M, Beyhl D, Görlich E, Al-Rasheid KAS, Marten I, Stierhof YD, Hedrich R, Schumacher K (2010) Arabidopsis V-ATPase activity at the tonoplast is required for efficient nutrient storage but not for sodium accumulation. Proc Natl Acad Sci USA **107:** 3251–3256

Leigh RA (2001) Potassium homeostasis and membrane transport. J Plant Nutr Soil Sci **164:** 193–198

Li HT, Liu H, Gao XS, Zhang H (2009) Knock-out of Arabidopsis AtNHX4 gene enhances tolerance to salt stress. Biochem Biophys Res Commun **382:** 637–641

Li P, Zhang G, Gonzales N, Guo Y, Hu H, Park S, Zhao J (2016) Ca^{2+}-regulated and diurnal rhythm-regulated Na^+/Ca^{2+} exchanger AtNCL affects flowering time and auxin signalling in Arabidopsis. Plant Cell Environ **39:** 377–392

Liu H, Tang R, Zhang Y, Wang C, Lv Q, Gao X, Li W, Zhang H (2010) AtNHX3 is a vacuolar K^+/H^+ antiporter required for low-potassium tolerance in Arabidopsis thaliana. Plant Cell Environ **33:** 1989–1999

Ma X, Zhang Q, Zhu Q, Liu W, Chen Y, Qiu R, Wang B, Yang Z, Li H, Lin Y, et al (2015) A robust CRISPR/Cas9 system for convenient, high-efficiency multiplex genome editing in monocot and dicot plants. Mol Plant **8:** 1274–1284

Ma YC, Augé RM, Dong C, Cheng ZM (2017) Increased salt tolerance with overexpression of cation/proton antiporter 1 genes: A meta-analysis. Plant Biotechnol J **15:** 162–173

Maathuis FJM, Sanders D (1995) Contrasting roles in ion transport of two K^+-channel types in root cells of Arabidopsis thaliana. Planta **197:** 456–464

Maathuis FJM, Ahmad I, Patishtan J (2014) Regulation of Na^+ fluxes in plants. Front Plant Sci **5:** 467

Martinoia E, Massonneau A, Frangne N (2000) Transport processes of solutes across the vacuolar membrane of higher plants. Plant Cell Physiol **41:** 1175–1186

Martinoia E, Maeshima M, Neuhaus HE (2007) Vacuolar transporters and their essential role in plant metabolism. J Exp Bot **58:** 83–102

Martinoia E, Meyer S, De Angeli A, Nagy R (2012) Vacuolar transporters in their physiological context. Annu Rev Plant Biol **63:** 183–213

Mäser P, Thomine S, Schroeder JI, Ward JM, Hirschi K, Sze H, Talke IN, Amtmann A, Maathuis FJM, Sanders D, et al (2001) Phylogenetic relationships within cation transporter families of Arabidopsis. Plant Physiol **126:** 1646–1667

McCubbin T, Bassil E, Zhang S, Blumwald E (2014) Vacuolar Na^+/H^+ NHX-type antiporters are required for cellular K^+ homeostasis, microtubule organization and directional root growth. Plants (Basel) **3:** 409–426

Murashige T, Skoog F (1962) A revised medium for rapid growth and bio assays with tobacco tissue cultures. Physiol Plant **15:** 473

Reguera M, Bassil E, Tajima H, Wimmer M, Chanoca A, Otegui MS, Paris N, Blumwald E (2015) pH regulation by NHX-type antiporters is required for receptor-mediated protein trafficking to the vacuole in Arabidopsis. Plant Cell **27:** 1200–1217

Schmid M, Davison TS, Henz SR, Pape UJ, Demar M, Vingron M, Schölkopf B, Weigel D, Lohmann JU (2005) A gene expression map of Arabidopsis thaliana development. Nat Genet **37:** 501–506

Spalding EP, Hirsch RE, Lewis DR, Qi Z, Sussman MR, Lewis BD (1999) Potassium uptake supporting plant growth in the absence of AKT1 channel activity: Inhibition by ammonium and stimulation by sodium. J Gen Physiol **113:** 909–918

Sze H, Chanroj S (2018) Plant endomembrane dynamics: Studies of K^+/H^+ antiporters provide insights on the effects of pH and ion homeostasis. Plant Physiol **177:** 875–895

Venema K, Quintero FJ, Pardo JM, Donaire JP (2002) The Arabidopsis Na^+/H^+ exchanger AtNHX1 catalyzes low affinity Na^+ and K^+ transport in reconstituted liposomes. J Biol Chem **277:** 2413–2418

Waese J, Fan J, Pasha A, Yu H, Fucile G, Shi R, Cumming M, Kelley LA, Sternberg MJ, Krishnakumar V, et al (2017) ePlant: Visualizing and exploring multiple levels of data for hypothesis generation in plant biology. Plant Cell **29:** 1806–1821

Walker DJ, Leigh RA, Miller AJ (1996) Potassium homeostasis in vacuolate plant cells. Proc Natl Acad Sci USA **93:** 10510–10514

Wang Y, Wu WH (2013) Potassium transport and signaling in higher plants. Annu Rev Plant Biol **64:** 451–476

Wu H, Zhang X, Giraldo JP, Shabala S (2018) It is not all about sodium: Revealing tissue specificity and signalling roles of potassium in plant responses to salt stress. Plant Soil **431:** 1–17

Yoshida K, Kondo T, Okazaki Y, Katou K (1995) Cause of blue petal color. Nature **373:** 291